JCI The Journal of Clinical Investigation

p53 suppresses lipid droplet-fueled tumorigenesis through phosphatidylcholine

Xiuduan Xu, … , Peng Li, Peng Jiang

J Clin Invest. 2024. https://doi.org/10.1172/JCI171788.

Research In-Press Preview Cell biology

Graphical abstract

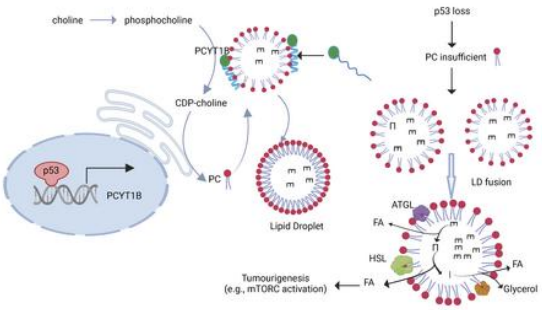

p53 suppresses lipid droplet-fueled tumorigenesis through phosphatidylcholine

Xiuduan Xu[1,2], Jianqin Wang[2], Li Xu[2], Peng Li[2,3,*], and Peng Jiang[1,2*]

[1] State Key Laboratory of Molecular Oncology School of Life Sciences, Tsinghua University, and Tsinghua-Peking Center for Life Sciences, Beijing 100084, China
[2] School of Life Sciences, Tsinghua University, and Tsinghua-Peking Center for Life Sciences, Beijing 100084, China
[3] Tianjian Laboratory of Advanced Biomedical Sciences, Zhengzhou University, Zhengzhou, China;
*Correspondence: P.L., li-peng@mail.tsinghua.edu.cn, Tel: 86-010-62797133; or P.J., pengjiang@tsinghua.edu.cn, Tel: 86-010-62786079

Conflict of interest: The authors have declared that no conflict of interest exists.

ABSTRACT

Choline deficiency causes disorders including hepatic abnormalities and is associated with an increased risk of multiple types of cancer(1, 2). Here, by choline free diet-associated RNA-seq analyses, we found that the tumor suppressor p53 drives the Kennedy pathway via PCYT1B to control the growth of lipid droplets (LDs) and their fueling role in tumorigenesis. Mechanistically, through upregulation of PCYT1B, p53 channeled depleted choline stores to phosphatidylcholine (PC) biosynthesis during choline starvation, thus preventing LD coalescence. Cells lacking p53 failed to complete this response to choline depletion, leading to hepatic steatosis and tumorigenesis, and these effects could be reversed by enforcing PCYT1B expression or restoring PC abundance. Furthermore, loss of p53 or defects in the Kennedy pathway increased surface localization of hormone-sensitive lipase (HSL) on LDs to release specific fatty acids that fueled tumor cells in vivo and in vitro. Thus, p53 loss leads to dysregulation of choline metabolism and LD growth, and couples perturbed LD homeostasis to tumorigenesis.

INTRODUCTION

Lipid droplets (LDs) serve as important organelles that primarily package neutral lipids, such as sterol esters or triglyceride (TG), for metabolic energy and membrane precursors with phospholipid monolayers decorated by LD-specific proteins(3, 4). In mammalian LDs, phosphatidylcholine (PC) is the major surface phospholipid and plays a crucial role in emulsifying LDs and regulating LD coalescence or fusion(5, 6). The main pathway for the synthesis of PC is the Kennedy (CDP-choline) pathway (Supplemental Figure 3B)(7), which is conserved from yeast to humans(8). LDs provide neutral lipid to lipoproteins for their maturation and secretion. In hepatocytes, ApoB lipidation is critical for the very low-density lipoproteins (VLDL) maturation and secretion, which directly controls plasma levels of TG and cholesterol. In addition to VLDL secretion, lipolysis also contributes to LDs-mediated mobilization of neutral lipids. HSL is a key enzyme in the mobilization of fatty acids from acylglycerols and can translocate from the cytosol to the surface of lipid droplets when stimulated to release specific fatty acids. Some of the proteins, such as the diacylglycerol acyltransferase 2 (DGAT2) and CIDE proteins, have been shown as LD-binding proteins that are essential for LD expansion (6, 9-11). Moreover, the LD localization of PCYT1A or PCYT1B (also known as CCTα and CCTβ respectively) allows for the local synthesis of sufficient PC to meet the demand for PC for LD surface expansion(5).

Choline is indispensable for many fundamental processes in the body, and its deficiency can cause reversible hepatic abnormalities in patients(12). Here, to elucidate how p53 loss confers mice with a more profound fatty liver in the absence of dietary choline, we performed RNA-seq analysis and found that the Kennedy pathway is highly dysregulated by p53 loss, contributing to LD coalescence and tumorigenesis. Mechanistically, through transcriptional up-regulation of PCYT1B expression, p53 efficiently channels depleted choline stores to PC synthesis during choline starvation, resulting in impaired LD coalescence and hepatic steatosis. Moreover, reduced PCYT1B expression or suppressed PC synthesis due to p53 loss increases the surface localization of HSL on LDs to release specific fatty acids as fuel for tumor cells in

vitro and in vivo using different hepatocellular carcinoma mouse models.

RESULTS

Choline-free diet-associated RNA-seq reveals downregulation of the Kennedy pathway in fatty liver of p53-deficient mice

Choline deficiency is associated with numerous disorders such as liver disease and atherosclerosis(13, 14). Here we happened to find that *p53*$^{-/-}$ mice showed robust sensitivity to choline starvation compared to *p53*$^{+/+}$ control mice. p53-deficient mice maintained on choline-free diet exhibited more severe fatty liver (Figure 1A). To investigate how this happens, we did RNA-seq analysis and compared gene expression profiles in the livers of *p53*$^{+/+}$ and *p53*$^{-/-}$ mice fed a choline-free diet. Interestingly, the expression levels of several genes, including Eda2r, Eif3j2, Pcyt1b and Upk3b, were mostly changed (Figure 1B and Supplemental Figure 1A). As with the increased fatty liver in p53-deficient mice induced by choline starvation, we were particularly interested in genes involved in lipid metabolism. We further compared the expression of genes involved in the regulation of lipid metabolism and found that Pcyt1b was the most significantly altered gene, with a strong decrease in expression in the livers of *p53*$^{-/-}$ mice (Figure 1C). Pcyt1b encodes an enzyme that converts phosphocholine to CDP-choline and is a rate-limiting enzyme in the Kennedy pathway (Figure 1D). Therefore, we focused on this metabolic pathway. Analysis of metabolites in this pathway independently confirmed the decrease in PCYT1B in *p53*$^{-/-}$ mice. Liver tissues from *p53*$^{-/-}$ mice showed higher levels of choline and phosphocholine (Figure 1E), and reduced PC as evidenced by decreased levels of propargyl-PC in *p53*$^{-/-}$ mice receiving propargyl-labelled choline (Figure 1F), compared to those from wild-type (WT) control animals. These observations suggest that low levels of PCYT1B in *p53*$^{-/-}$ tissues limit the metabolic step it catalyzes, leading to an accumulation of upstream metabolites and a reduction in downstream PCs during choline restriction. Intriguingly, no changes in citicoline levels were observed (Figure 1E), which may be due to compensatory effects of other metabolic pathways. Together, these findings reveal a reduced Kennedy pathway in the fatty liver of p53-deficient mice in the absence of dietary choline.

p53 drives the Kennedy pathway for de novo PC biosynthesis

Similar to the findings observed in mice (Figure 1, E and F), metabolomics analysis revealed that p53 ablation in HepG2 cells resulted in an accumulation of cellular choline and phosphocholine and reduced levels of the downstream PC, while citicoline remained unchanged when cells were cultured in choline-free medium (Supplemental Figure 1, B and C), indicating a possible role for p53 in modulating the Kennedy pathway. Notably, treatment of cells or mice with choline minimizes the difference in levels of PC in WT and p53-deficient situations (Supplemental Figure 1, D-F), despite that supplying cells with choline led to overall elevation of cellular PC abundance (Supplemental Figure 1G), indicating that exogenous choline supplementation could compromise the effect of p53 on PC metabolism.

We then performed a ^{13}C metabolic flux analysis. By culturing cells with [1, 2-$^{13}C_2$]choline, we observed that p53 loss resulted in a reduction in the synthesis of phosphocholine, citicoline and PC from choline (Figure 2, A-C). Intriguingly, lower levels of ^{13}C-labeled choline were found in *p53*$^{-/-}$ cells, raising a possibility that p53 might promote choline uptake (Figure 2B,

left). Nevertheless, these data suggest that p53 deficiency impairs PC biosynthesis. In supporting of this, in vivo flux by treating mice with propargyl-labelled choline revealed significantly higher levels of propargyl-PC in liver tissue from $p53^{+/+}$ mice compared to $p53^{-/-}$ mice (Figure 1F). Similar results were also obtained in HepG2 cells (Supplemental Figure 1H).

The highly active PC synthesis within p53WT cells indicate that these cells might be susceptible to choline starvation. Indeed, choline depletion strongly dampened the survival of p53WT cells, while feasibly affected p53-deficient cells (Supplemental Figure 2, A and B). Notably, addition of exogenous choline or PC totally reversed this effect (Supplemental Figure 2, A and B). Similar findings were also found in the soft agar assays. Supplying cells with a choline-free medium resulted in a decreased anchorage-independent growth of $p53^{+/+}$, but not $p53^{-/-}$, HepG2 cells in soft agar, and either choline or PC supplementation completely restored the growth of $p53^{+/+}$ cells (Supplemental Figure 2, C and D). In agreement with the metabolic data (Supplemental Figure 1, C-E), no significant difference in the survival of $p53^{+/+}$ and $p53^{-/-}$ cells was observed when choline or PC was sufficient (Supplemental Figure 2E).

Collectively, these findings suggest p53 positively regulates the Kennedy pathway and that cells with wild-type p53 are dependent on choline or PC for survival.

p53 transcriptionally upregulates PCYT1B expression

Next, we investigated how p53 regulates de novo PC biosynthesis. Consistent with the RNA-seq data (Figure 1, B and C), loss of p53 was associated with decreased mRNA and protein levels of PCYT1B in mouse liver and HepG2 cells under both choline-deficient and choline-sufficient conditions (Figure 2, D-G). Moreover, results from immunohistochemistry showed that the protein expression of PCYT1B was higher in $p53^{+/+}$ murine livers, and merely expressed in liver tissues of $p53^{-/-}$ mice (Figure 2H). In line with these expression data, $p53^{-/-}$ cells displayed lower cellular PCYT1 activity than that in their wild-type counterparts (Figure 2I). Additionally, PCYT1B expression was lower in several tissues except heart and brain in $p53^{-/-}$ mice than $p53^{+/+}$ mice (Supplemental Figure 3A).

We further used chemical reagents to activate p53. Pharmacological activation of p53 with doxorubicin (DOX) boosted the expression of PCYT1B in $p53^{+/+}$ HepG2 cells, while modestly in $p53^{-/-}$ HepG2 cells (Supplemental Figure 3, B-D). By comparison, the expression of the other enzymes within these pathways were not dramatically changed (Supplemental Figure 3C). We also generated a tetracycline-controlled (Tet-On) inducible system, and found that induction of p53 resulted in an increase in PCYT1B expression (Supplemental Figure 3, E and F). These findings were also supported by the observation that DOX, etoposide (ETO), or a MDM2 antagonist, nultin-3, increased PCYT1B expression in a dose- and time-dependent manner in different types of cells (Supplemental Figure 4, A-I). Consistently, knockout of p53 downregulated the expression of PCYT1B, and the effect of Nutlin-3 or ETO on PCYT1B expression was totally blocked when p53 was absent (Supplemental Figure 5, A-C). These findings indicate that regulation of PCYT1B is p53 dependent.

By analyzing the genomic sequences of *PCYT1B* gene, we identified two putative p53 response elements in mouse *Pcyt1b* gene and three putative p53 response elements in human *PCYT1B* gene (Supplemental Figure 5, D and E). Chromatin immunoprecipitation (ChIP) assays revealed that endogenous p53 bound to the genomic regions containing these response elements, and this effect could be enhanced by Choline starvation in mouse liver (Figure 2J).

Similar results were obtained in HepG2 cells, where p53 occupancy of these response elements was found and DOX treatment strongly enhanced this effect (Supplemental Figure 5F). Likewise, Flag-p53 was found to associate with the PCYT1B genomic DNA when expressed in HEK293 cells (Supplemental Figure 5G). In reporter assays, luciferase expression driven by genomic regions of PCYT1B containing these response elements (RE1, RE2 or RE3) increased luciferase expression in response to p53 introduction, whereas mutant REs abolished this effect (Figure 2K).

p53 is the most frequently mutated gene in human cancer. To investigate whether PCYT1B expression can be also influenced by tumor-associated mutant p53, we knocked down p53 expression in MDA-MB-231 cells (carrying the p53R280K mutation) and DU145 cells (heterozygous p53P223L/V274F) via siRNA interference. Unlike wild-type p53, mutant p53 ablation showed minimal effect on PCYT1B expression in these cell lines (Supplemental Figure 5, H and I). Furthermore, ectopic expression of mutant p53 (R175 or R273H) in p53-deficient HCT116 cells also did not significantly alter the expression of PCYT1B (Supplemental Figure 5, J and K).

p53 impairs hepatic steatosis when choline is scarce

Next, we considered the possibility that activation of PCYT1B-PC axis by p53 might explain its role in suppressing hepatic steatosis. To this end, we generated liver-specific PCYT1B knockdown mice (Figure 3A, and Supplemental Figure 6A), and found that PCYT1B downregulation resulted in an increase in lipid accumulation in the livers and developed a fatty liver phenotype (Figure 3B). Consistently, higher content of intrahepatic TG, but not plasma TG, was observed in shPCYT1B mice compared to control shLacZ mice (Figure 3, C and D). Moreover, PCYT1B ablation led to a significant decline in PC levels in liver tissue, further demonstrating the physiological importance of PCYT1B for PC biosynthesis (Figure 3E), which also raised the possibility that PC may be essential for PCYT1B-mediated suppression of lipid accumulation in the liver. Indeed, restoration of PC levels by dietary PC strongly reversed the accumulation of lipid as well as TG induced by choline starvation in the liver, and minimized the difference between control mice and PCYT1B-knockdown mice (Figure 3, B, C and E).

Notably, PCYT1B knockdown did not affect the weight of animal body and liver (Supplemental Figure 6B). In agreement with the lipid accumulation data (Figure 3, B and C), shPCYT1B mice did to some extent show higher frequency of liver dysfunction (raised AST, ALT and ALP), and this effect could be totally blocked by PC addition (Supplemental Figure 6C). We also confirmed these findings by overexpression of PCYT1B in liver of $p53^{-/-}$ mice fed on choline-deficient diet (Figure 3F, and Supplemental Figure 6D). In keeping with the knockdown data (Figure 3, A-E), overexpression of PCYT1B expression led to a reduction in contents of liver lipid and TG (not plasma TG), and correspondingly increased PC abundance (Figure 3, G-J, and Supplemental Figure 6E). By contrast, PCYT1B overexpression had no significant effect on body and liver weight or liver function (Supplemental Figure 6, F and G). These findings reveal PCYT1B limits hepatic steatosis via supporting PC biosynthesis.

Additionally, immunohistochemical analysis showed that dietary administration of PC reduced the lipid content in the liver of $p53^{-/-}$ mice, and narrowed the difference between $p53^{+/+}$

and *p53*$^{-/-}$ mice (Figure 3, K and L, and Supplemental Figure 7, A and B). Similar results were also obtained from transmission electron microscopy (TEM) scanning analysis of liver tissues (Figure 3M). Analysis of TG levels showed that the increased liver TG caused by p53 deficiency was abolished by PC administration, and these findings were further supported by the observations that intrahepatic PC in *p53*$^{-/-}$ mice was restored by dietary PC (Figure 3, N-P). In keeping with the PCYT1B KD and overexpression data (Supplemental Figure 6), PC-supplemented diet did not change the weight of murine body and liver (Supplemental Figure 7, C and D). Like PCYT1B KD, p53 loss caused increased activities of AST, ALT and ALP, which was completely abrogated by PC addition (Supplemental Figure 7, E-G). Moreover, given that there is no difference in body weight of *p53*$^{+/+}$ and *p53*$^{-/-}$ mice on choline-free diet, p53 deficiency did not affect the body composition (Supplemental Figure 7, H and I). Additionally, levels of blood glucose were not changed between *p53*$^{+/+}$ and *p53*$^{-/-}$ mice (Supplemental Figure 7J). Again, along with the metabolic data in the situation of choline supplementation (Supplemental Figure 1, C-E), dietary choline-treated mice did not develop fatty liver, and there were no differences in liver dysfunction, body weight or liver weight between *p53*$^{+/+}$ and *p53*$^{-/-}$ mice (Figure 1A, and Supplemental Figure 7, K-N). Collectively, these findings suggest upregulation of PCYT1B by p53 represses NAFLD development via PC during choline starvation.

p53 suppresses LD coalescence via PCYT1B-mediated PC synthesis during choline starvation

LDs are the defining feature of hepatic steatosis and lipid storage(15). After treatment with oleate, *p53*$^{-/-}$ HepG2 cells displayed larger droplets than *p53*$^{+/+}$ cells when choline was deprived (Figure 4A). Moreover, by time-lapse confocal microscopy, we observed visible droplet coalescence and size growth in *p53*$^{-/-}$ cells, but not in *p53*$^{+/+}$ cells (Supplemental Movie 1 and 2), suggesting that p53 inhibits LD coalescence. To investigate whether this role of p53 is mediated by PCYT1B, we compared the size of LDs by BODIPY staining and TG levels in oleate-loaded cells treated with Miltefosine, a PCYT1A/B inhibitor. Miltefosine treatment led to the formation of large droplets, and minimized the difference between *p53*$^{+/+}$ and *p53*$^{-/-}$ cells (Supplemental Figure 8A). Given that PCYT1A is not regulated by p53 (Supplemental Figure 3C), these findings indicate that activation of PCYT1B contributes to p53-mediated suppression of LD growth in size. We also confirmed this by generating cell lines with stable overexpression of PCYT1B (Figure 4B, left). Forced expression of PCYT1B visually reduced cellular size of LDs, decreased the TG levels and correspondingly led to a significant increase in PC levels in both *p53*$^{+/+}$ and *p53*$^{-/-}$ cells when oleate was loaded (Figure 4B, and Supplemental Figure 8B). Notably, overexpressed PCYT1B showed colocalization with LDs (Supplemental Figure 8C), and translocation of PCYT1B to the droplet surface is thought to be able to impede LD size by locally providing adequate PC(16). In line with this, we observed strong colocalization of endogenous PCYT1B and LDs in *p53*$^{+/+}$ cells, whereas larger LDs were observed in *p53*$^{-/-}$ cells with attenuated co-localization of PCYT1B due to reduced expression of PCYT1B (Figure 4C). Hence, p53 inhibits LD coalescence by upregulating surface levels of PCYT1B on LDs during choline starvation.

We further wanted to know whether the regulation of LD coalescence by p53 is PC-dependent. p53 depletion led to significant reduction in PC levels in murine liver tissues (Figure

1F, 2C, 3P, and Supplemental Figure 8B), and oleate- or palmitic acid (PA)-loaded HepG2 cells (Supplemental Figure 9, A and B). Interestingly, addition of PC decreased LD size in both $p53^{+/+}$ and $p53^{-/-}$ cells loaded with oleate, and abolished the difference between them (Figure 4D). These results were further confirmed by transfecting cells with liposomal PC (Supplemental Figure 9C). Consistent with the finding that p53 suppresses LD coalescence mentioned above, although the LD contents and TG contents increased when p53 was knockout, the number of LDs declined in $p53^{-/-}$ cells (Figure 4, D, E and F). Notably, these phenomena were not observed when cells were supplied with PC (Figure 4, D, E and F). These findings indicate increased PC synthesis is required for p53-mediated suppression of LD calescence during choline starvation. To confirm these findings and also to visualize and compare the size of LDs, we further employed electron microscopy strategies. Similarly, $p53^{-/-}$ cells had larger LDs, and PC addition strongly reduced the size of LDs in both $p53^{+/+}$ and $p53^{-/-}$ cells loaded with oleate (Figure 4G). These findings were further confirmed by means of electron microscopic 3D reconstruction methods. $p53^{-/-}$ cells had larger lipid droplets present, and this effect was blocked by PC treatment (Supplemental Figure 9D), reinforcing the notion that p53 regulates LD coalescence by modulating PCYT1B-mediated PC synthesis.

LDs provide lipid for VLDL secretion and FAs for oxidation. Therefore, lowering of either of these two events would expectedly cause LD growth (providing more surface area). However, levels of plasma TG in $p53^{-/-}$ mice maintained on choline-free diet were not significantly different from those in wild-type mice (Figure 3O), and $p53^{+/+}$ and $p53^{-/-}$ mice treated with Triton WR-1339, a potent inhibitor of VLDL-TG catabolism(17), displayed comparable levels of plasma TG (Supplemental Figure 9E). Consistently, the secretion rates of ApoB-100 and ApoB-48 in the presence of Triton WR-1339 were similar between wild-type and $p53^{-/-}$ mice (Supplemental Figure 9F), and the expression of ApoB in the murine livers were not affected by p53 knockout, or PC treatment (Supplemental Figure 9G). Moreover, we did not observe any change in the activity of DGAT1(diacylglycerol O-acyltransferase 1), which reflects the VLDL secretion and particle size(18) (Supplemental Figure 9H). Thus, it appears that regulation of LD size growth by p53 may not due to VLDL secretion.

Also, we examined the effect of p53 and PCYT1B on lipolysis, which presumably can induce the break-up of larger droplets into smaller ones to provide more surface area for lipases(16, 19). By inducing LD formation followed by induction of lipid mobilization with serum-free medium lacking oleate, we found that wild-type control HepG2 cells had much few droplets, and by contrast, many droplets remained in $PCYT1B^{-/-}$ cells or $p53^{-/-}$ cells (Figure 4H). In line with this, highly increased levels of cellular glycerol, a production of lipolysis, was observed in wild-type control cells, not in the knockout cells (Figure 4I). Therefore, these findings together indicate p53 controls LD size by orchestrating LD coalescence and lipolysis via regulating PCYT1B-mediated PC biosynthesis.

PCYT1B is a tumor suppressor and metabolic enzyme activity is required for its tumor suppressive capacity

By comparing the expression of PCYT1B in human hepatocellular carcinoma of different grades and in normal tissues, we found that expression of this enzyme was significantly high in normal tissues, but was strongly declined in high-grade tumors, negatively correlating with tumor progression (Figure 5A). Moreover, decreased PCYT1B expression was significantly

correlated with a poor patient survival (Figure 5B), suggesting that PCYT1B may play a role in suppressing tumor development.

To explore the effect of PCYT1B on tumorigenesis, we established a HCC model(20), in which $p53^{fl/fl,alb\text{-}cre}$ mice fed on choline-deficient diet were co-injected with the MYC oncogene along with PT3 plasmid DNA expressing PCYT1B or GFP control (Figure 5C). PCYT1B-injected mice showed a reduction in tumor burden in the liver and increased survival rate (Figure 5, D and E). The mTORC signaling pathway is a major determinant of tumorigenesis and can be activated by sufficient fatty acids(21, 22). Consistently, a strong reduction in tumor proliferative activity and mTORC1 signaling activity were observed in PCYT1B-overexpressing mice (Supplemental Figure 10, A and B), with a decrease in LDs and TG content and a corresponding increase in PC abundance in the liver (Figure 5, F-H). Notably, by measuring the size of LDs and tumors in the livers of all treated mice, we found a significant positive correlation between LD size and tumor size (Figure 5I). The body and liver weights, plasma TG, as well as blood glucose of mice injected with PCYT1B did not change significantly, except for a decrease in ALT levels (Supplemental Figure 10, C-E). Also, we used diethylnitrosamine (DEN) combined with carbon tetrachloride (CCl_4) (DEN-CCl_4) to establish another liver cancer model in $p53^{fl/fl,alb\text{-}cre}$ mice fed on choline-deficient diet to confirm the tumor-suppressive ability of PCYT1B (Supplemental Figure 10, F and G). Similarly, in this system, liver-specific overexpression of PCYT1B (Ad-PCYT1B) did not alter body and liver weight, but significantly reduced both the number and size of tumors (Supplemental Figure 10, H and I). And, a strong decrease in proliferative effect was observed in PCYT1B-overexpressed tumors (Supplemental Figure 10, J and K). Moreover, PCYT1B overexpressed liver tissues displayed increased PC levels and correspondingly reduced TG and lipid contents (Supplemental Figure 10, L-N). Again, we found that the size of LDs positively correlated with tumor size in these mice (Supplemental Figure 10O). In addition, PCYT1B overexpression did not change plasma TG and blood glucose, and to some extent affected liver function (Supplemental Figure 10, N, P and Q). Thus, these results suggest PCYT1B acts as a tumor suppressor.

We next investigated whether the enzymatic activity of PCYT1B is required for its tumor suppressive function. We injected $p53^{fl/fl,alb\text{-}cre}$ mice with constructs expressing MYC oncogene along with GFP control, wild-type PCYT1B, or enzymatic activity-dead mutant PCYT1B bearing K122R mutation or M domain depletion (ΔMD) (Supplemental Figure 11, A and B). Compared to mice injected with wild-type PCYT1B, neither PCYT1B-K122R- nor PCYT1B-ΔMD-expressing mice showed an inhibitory ability for tumorigenesis (Figure 5, J and K, and Supplemental Figure 11C); and indeed, no increase in the enzymatic activity of PCYT1 was observed in the tumors of these mice (Figure 5L). Consistent with this, K122R mutation or M domain depletion (ΔMD) totally blocked the ability of PCYT1B to modulate PC, TG and lipid contents (Figure 5, L-O). As could be expected, mice expressing these PCYT1B mutants in the liver showed no change in body and live weight or liver function (Supplemental Figure 11, D-F).

Collectively, these findings suggest that PCYT1B is a tumor suppressor whose enzymatic activity is indispensable for its tumor suppressive capability.

PC availability suffices for p53-mediated tumor suppression

To determine the tumor suppressive effect of PC, we injected $p53^{fl/fl}$ mice constructs expressing the MYC oncogene and treated the mice with PC in the presence of a choline-deficient diet (Supplemental Figure 12A). PC administration led to increased levels of intrahepatic PC, and did not affect the body and liver weight of the mice (Supplemental Figure 12, B and C). Notably, PC-treated mice exhibited suppressed tumor incidence and proliferative activity, and decreased LDs and TG content in the liver (Supplemental Figure 12, D-G). Like PCYT1B overexpression, PC treatment improved the liver function as indicated by the reduction in ALT activity (Supplemental Figure 12H). Consistent with this, lower PC levels in the liver of liver-specific knockout PCYT1B mice decreased tumor burden, TG levels and mTORC signaling in the liver, while PC administration abolished these effects (Supplemental Figure 13, A-F).

We next investigated if PC is necessary for p53-mediated tumor suppression. Compared to p53 wild-type mice, $p53^{fl/fl,alb\text{-}cre}$ mice developed liver tumors larger and at higher frequency in the setting of DEN-CCl_4 treatment and choline-free diet (Figure 6, A-C, and G). Strikingly, PC administration restricted tumorigenesis and minimized the difference between $p53^{+/+}$ and $p53^{-/-}$ mice (Figure 6, A-C, and E). Moreover, increased tumor proliferative activity and cellular mTORC1 signaling, as well as LD and TG contents in the liver produced by p53 loss were all reversed by PC treatment (Figure 6D, and Supplemental Figure 13, G-I). In the system, LD size was also significantly correlated with tumor size (Figure 6, E and F). No obviously change in body and liver weight, as well as plasma TG and blood glucose were observed, but interestingly, PC treatment reversed the liver dysfunction of $p53^{-/-}$ mice (Supplemental Figure 13, J-L). In addition, $p53^{-/-}$ mice exhibited constitutive low expression of PCYT1B before and after the onset of tumors induced by DEN, suggesting that down-regulation of PCYT1B is compatible with tumor initiation in the absence of p53 and may facilitate tumorigenesis from an early time (Supplemental Figure 14, A and B). Collectively, these data suggest that blockade of PC synthesis contributes to the development of p53-deficient liver tumors.

LDs support tumor growth in vivo

We then were curious to see if LDs could also support tumor growth in vivo, especially those derived from p53-deficient mice fed a choline-free diet. To this end, lipid droplets were isolated and purified from the equal amount of liver tissue from mice fed on a choline-deficient diet and then injected into the transplanted tumor, a strategy that allows a crude comparison of the direct effect of lipid droplets on tumor growth (Figure 6G). Strikingly, intratumoral injection of LDs promoted tumor growth, whereas those isolated from $p53^{-/-}$ liver had a more profound effect (Figure 6, H-J). Western blot analysis revealed that tumors with exogenous LD supplementation exhibited increased mTORC signaling activity, and consistently, even higher levels of mTORC signaling activity were observed in tumors receiving $p53^{-/-}$ LDs (Figure 6K). Thus, these results suggest that lipid droplets can support tumor growth and that p53-deficient liver-derived lipid droplets appear to have a stronger effect.

Defects in the p53-PCYT1B-PC axis increase the surface localization of HSL on LDs to release specific fatty acids

We also wanted to know why or how LD growth induced by p53 inactivation accompanies tumorigenesis during choline starvation. Preventing endoplasmic reticulum (ER) stress by LDs

is thought to help tumor cells survive (23). However, p53 knockout had minimal effect on the activation of the ER stress response, as measured by the expression of XBP1s/XBP1u and the ER chaperone Bip in choline-starved HepG2 cells, even during OA stimulation (Supplemental Figure 14, C and D). Similarly, no differences in Bip mRNA levels in the liver were observed between $p53^{+/+}$ and $p53^{-/-}$ mice fed on a choline-free diet (Supplemental Figure 14E), suggesting that improving ER homeostasis is not the underlying mechanism (s).

Interestingly, metabolomic analysis revealed a strong accumulation of six specific free fatty acids 16:0, 18:0, 18:1, 18:2, 20:4 and 22:6 in the liver interstitial fluid of PCTY1B-knockdown mice (Figure 7A). Strikingly, the loss of p53 consistently led to the accumulation of these six specific free fatty acids (FFAs) in the liver interstitial fluid, and PC administration completely abolished this phenomenon (Figure 7B, and Supplemental Figure 14F). Therefore, it is likely that LD growth induced by defects in the p53-PCYT1B-PC axis fuels tumor cells by providing specific free fatty acids. p53 did not affect the expression of genes involved in FFA uptake in tumor cells (Supplemental Figure 14, G and H). Next, we were curious about how LD growth alters FFA levels in the microenvironment. The increase in surface area of LD and decrease in PC synthesis induced by p53 loss or inhibition of the Kennedy pathway may increase the surface localization of certain lipases on LD to generate fatty acids (FAs), which are released as fuel for tumors. To test this possibility, we fractioned mouse liver tissues and purified LDs. Interestingly, higher levels of HSL were found in the LD fraction of shPCYT1B-silenced livers, and confocal imaging analysis further revealed more HSL on the LD surface when PCYT1B was knocked down (Figure 7C). ATGL and HSL are the major lipases that are functionally localized to LDs (24). By contrast, LD localization of ATGL was not altered by PCYT1B ablation (Figure 7C). Consistently, p53 knockout resulted in a strong increase in HSL, but not in other lypases on LDs in mouse liver and hepatocytes (Figure 7D). When PC was sufficient, this effect disappeared (Figure 7D). In line with the effect of PCYT1B depletion or p53 knockout on FFAs, inhibition of HSL reduced the levels of the six FFAs in liver interstitial fluid and minimized the difference between $p53^{+/+}$ and $p53^{-/-}$ mice (Figure 7E). Likewise, depletion of PCYT1B or p53 in hepatocytes increased extracellular FFA levels, whereas HSL inhibition or PC supplementation reduced FFA secretion (Supplemental Figure 14I). Thus, p53 loss or defects in the Kennedy pathway increases surface localization of HSL on LDs for releasing specific FFAs. These findings were further strengthened by the observations that loss of p53 did not alter either protein or mRNA expression of HSL (Figure 7, C and D, and Supplemental Figure 14J).

FAs released by HSL fuel tumorigenesis in p53-deficient mice

We further investigated the effect of HSL on tumorigenesis using an HCC model(20) by injecting mice with the MYC oncogene along with CRISPR plasmid DNA expressing cas9 and sgRNAs targeting Axin1(Supplemental Figure 15A). In agreement with the fatty acid data (Figure 7E), HSL inhibition blunted the tumor burden and proliferation of tumor cells in the liver of $p53^{-/-}$ mice (Supplemental Figure 15, B and C). Notably, $p53^{-/-}$ tumors exhibited higher mTORC activity compared to $p53^{+/+}$ tumors, and HSL inhibition strongly attenuated this phenomenon in both tumor types (Supplemental Figure 15D). Consistently, liver-specific knockdown of HSL reduced the number and proliferative activity of tumors in the liver of $p53^{-/-}$ mice (Figure 7F, and Supplemental Figure 15, E and F), and strongly impended mTORC

activity in both $p53^{+/+}$ and $p53^{-/-}$ tumors (Figure 7G). In contrast, injection of HSL sgRNA had no effect on LD levels (Figure 7H), supporting the notion that HSL acts downstream of LD growth to influence tumor development.

We also extended these findings to in vitro cell culture systems. Culturing with shPCYT1B or p53-dificient liver interstitial fluid significantly promoted HepG2 cell proliferation and mTORC activation in these tumor cells (Supplemental Figure 16, A-F). Similar findings were obtained using shPCYT1B or p53-dificient hepatocyte-conditioned medium to culture tumor HepG2 cells (Figure 7, I and J, and Supplemental Figure 16, G-K). CD36 is a major player in the fatty acid uptake in metabolic tissues(25). Blocking FA uptake by addition of CD36 inhibitor completely abolished HepG2 cell proliferation induced by culture with PCYT1B-silenced or p53-deficient liver interstitial fluid or hepatocyte-conditioned medium (Supplemental Figure 16, A, H and I), suggesting the importance of microenvironmental FAs in fueling tumor cell proliferation. Consistent with the abovementioned findings, culture with liver mesenchyme from mice treated with PC or HSL inhibitor, or with conditioned medium from hepatocytes treated with PC or HSL inhibitor, resulted in suppressed proliferation of HepG2 cells and reduced mTORC activity of tumor cells (Figure 7, I and J, and Supplemental Figure 16, B, C, E, F, J and K). Notably, proliferation and mTORC activity of cells cultured in conditioned media of HSL-inhibited hepatocytes was largely restored upon further addition of oleic acid (OA; 18:1) (Figure 7, I and J), reinforcing the notion that FAs support tumor cell proliferation induced by p53 deletion or the Kennedy pathway defects.

DISSCUSSION

Here, we identify a role for p53 in lipid droplet biology and metabolic fueling of tumors by LD growth through the Kennedy pathway regulation (Supplemental Figure 17A). Coupled with the finding that choline starvation promotes LD growth and liver lipid accumulation in the absence of p53, we observed increased lipid droplet accumulation associated with tumorigenesis in p53-deficient mice, and PC restoration was able to inhibit tumor burden. In order to functionally explore the contribution of the Kennedy pathway in the early stages of p53-mediated tumor suppression, we also looked at changes in PCYT1B expression after DEN treatment but before the onset of frank tumors or after tumor onset in choline-free diet mice. $p53^{-/-}$ mice showed persistently low expression of PCYT1B before and after tumor onset, compared to $p53^{+/+}$ mice. Moreover, low expression of PCYT1B was accompanied by a corresponding increase in LD accumulation, suggesting that inhibition of PCYT1B is compatible with tumor initiation in the absence of p53 and may promote the accumulation of LDs in normal hepatocytes that facilitate tumorigenesis from an early time.

Under certain conditions of nutrient stress, the hydrolysis of lipid droplets is thought to be associated with cancer cell survival and may function as a storage of cellular excess of lipid molecules to counteract stress. However, cancer cells usually contain large amounts of LDs, and how this happens is still a mystery. Some studies suggest LDs may protect tumor cells either by improving ER homeostasis or by acting as scavengers of reactive oxygen species (ROS) in tumor cells (26). Unexpectedly, here we found that during choline starvation, LD growth induced by p53 loss-mediated suppression of the Kennedy pathway can actually increase the surface localization of HSL on LDs to release FAs as fuel for tumorigenesis. And the exact role of LD in tumorigenesis needs further investigation.

Since HSL, but not ATGL, alters the levels of some specific fatty acids, it is possible that these fatty acids are derived from cholesteryl esters. Direct LC-MS analysis of liver tissue from mice on a choline-deficient diet showed that certain cholesteryl esters were reduced in p53-deficient or PCYT1B-depleted liver tissues. Furthermore, these cholesteryl esters were mostly enriched in the same six fatty acyl chains found in the specific fatty acids, and PC treatment restored the levels of these cholesteryl esters (Supplemental Figure 17, B and C). It is therefore likely that these specific fatty acids are produced by the hydrolysis of cholesteryl esters.

HCC is a particularly challenging tumor with no effective therapies or druggable drivers. Consistent with our observations, human liver tumors with reduced expression of PCYT1B, like those with p53 loss, are associated with poor prognosis and patient survival, suggesting the therapeutic potential of targeting the Kennedy pathway for potential prevention of p53-deficient liver tumors. Together with this, our findings reveal a role for p53 in the regulation of LD growth, provide insights into the understanding of the physiological functions of p53, and have theoretical implications for the clinical treatment of p53 mutant tumors as well as other human diseases associated with excessive lipid storage mediated by LDs.

Methods

Sex as a biological variable. Our study exclusively examined male mice. It is unknown whether the findings are relevant for female mice.

Semi-quantitative RT–PCR and quantitative RT–PCR. Briefly, total RNA was isolated from triplicate wells in each condition using Total RNA purification Kit (GeneMark, TR01) and 2 μg RNA of each sample was reversed to cDNA by First-strand cDNA Synthesis System (Thermo scientific, K1621). 0.04 μg cDNA product of each sample was used as template to conduct semi-quantitative or quantitative PCR. qPCR was performed on CFX96 Real-Time PCR System (Bio-Rad, USA) and the amplifications were done using the SYBR Green PCR Master Mix (Gene star, A112-100). The fold changes of gene expression were calculated after being normalized to ACTB. The primers used in this study are listed in **Supplemental Table 1.**

^{13}C-labeled choline tracer studies. *p53*$^{+/+}$ and *p53*$^{-/-}$ HepG2 cells were cultured in choline free medium for 12 hours. The medium was then removed and substituted for choline free medium supplemented 200 μM [1,2-$^{13}C_2$] choline (Cambridge Isotopes, CLM-548-0.1) for a further 30 minutes. The cells were washed twice with PBS, then related metabolites were extracted and analysis by LC-MS (*see Supplemental Methods for details*).

Statistical analysis. No statistical methods were used to predetermine sample size. All the results are shown as means ± SD. All statistical methods used were specified in the figure legends. All statistical analysis was performed, and P values were obtained using the Graph Pad Prism software 7.0 (Graph Pad Software, Inc. USA). An unpaired two-tailed Student's t-test (two-sided ANOVA) was used to calculate the *P* values, except specified otherwise. $P< 0.05$ was considered significant. $*P < 0.05$, $**P< 0.01$, $***P < 0.001$, n.s. not significant.

Study approval. All mice were maintained under specific pathogen-free conditions and used in accordance with protocols approved by the Institutional Animal Care and Use Committees of Tsinghua University for animal welfare. The laboratory animal facility has been licensed by the IACUC.

Data availability. All data supporting the findings of this study are included in this article or in the Supplemental Supporting Data Values file. No new code or algorithms were generated. The accession number for the RNA-Seq data reported in this study are deposited in the NCBI's BioProject database, BioSample: SAMN37571050, SAMN37571051, SAMN37571052, SAMN37571053, SAMN37571054, SAMN37571055, respectively. Materials generated by the authors and used in this study are available from the corresponding authors on reasonable request.

Author contributions

X.X., P.L. and P.J. designed the experiments. X.X. performed all of the experiments, collected and analyzed the data. Q.W. and L.X. provided technical assistance. P.L. and P.J. supervised the research, and P.J. interpreted the data and wrote the manuscript. All authors commented on the manuscript.

Acknowledgements

We thank Drs. Suneng Fu, Xun Lan, Xuerui Yang, Ning Li and Chang Liu for technical assistance. We thank Xiaohui Liu and Weihua Wang for helping with the LC-MS/MS experiments. This research was supported by the National Natural Science Foundation of China (82125030, 82341022 and 81930082 to P.J.), National Key R&D Program of China (2018YFA0506900 to P.L.), and National Natural Science Foundation of China (92157107 to L.X.)

References

1. Zeisel SH, and Blusztajn JK. Choline and human nutrition. *Annu Rev Nutr.* 1994;14:269-96.
2. Ueland PM. Choline and betaine in health and disease. *J Inherit Metab Dis.* 2011;34(1):3-15.
3. Walther TC, and Farese RV, Jr. Lipid droplets and cellular lipid metabolism. *Annu Rev Biochem.* 2012;81:687-714.
4. Gluchowski NL, Becuwe M, Walther TC, and Farese RV, Jr. Lipid droplets and liver disease: from basic biology to clinical implications. *Nat Rev Gastroenterol Hepatol.* 2017;14(6):343-55.
5. Krahmer N, Guo Y, Wilfling F, Hilger M, Lingrell S, Heger K, et al. Phosphatidylcholine synthesis for lipid droplet expansion is mediated by localized activation of CTP:phosphocholine cytidylyltransferase. *Cell Metab.* 2011;14(4):504-15.
6. Barneda D, and Christian M. Lipid droplet growth: regulation of a dynamic organelle. *Curr Opin Cell Biol.* 2017;47:9-15.

7. Kennedy EP, and Weiss SB. The function of cytidine coenzymes in the biosynthesis of phospholipides. *J Biol Chem.* 1956;222(1):193-214.
8. McMaster CR. From yeast to humans - roles of the Kennedy pathway for phosphatidylcholine synthesis. *FEBS Lett.* 2018;592(8):1256-72.
9. Stone SJ, Levin MC, Zhou P, Han J, Walther TC, and Farese RV, Jr. The endoplasmic reticulum enzyme DGAT2 is found in mitochondria-associated membranes and has a mitochondrial targeting signal that promotes its association with mitochondria. *J Biol Chem.* 2009;284(8):5352-61.
10. Bartz R, Li WH, Venables B, Zehmer JK, Roth MR, Welti R, et al. Lipidomics reveals that adiposomes store ether lipids and mediate phospholipid traffic. *J Lipid Res.* 2007;48(4):837-47.
11. Gong J, Sun Z, Wu L, Xu W, Schieber N, Xu D, et al. Fsp27 promotes lipid droplet growth by lipid exchange and transfer at lipid droplet contact sites. *J Cell Biol.* 2011;195(6):953-63.
12. Buchman AL, Dubin MD, Moukarzel AA, Jenden DJ, Roch M, Rice KM, et al. Choline deficiency: a cause of hepatic steatosis during parenteral nutrition that can be reversed with intravenous choline supplementation. *Hepatology.* 1995;22(5):1399-403.
13. Zeisel SH, and da Costa KA. Choline: an essential nutrient for public health. *Nutr Rev.* 2009;67(11):615-23.
14. Goh YQ, Cheam G, and Wang Y. Understanding Choline Bioavailability and Utilization: First Step Toward Personalizing Choline Nutrition. *J Agric Food Chem.* 2021;69(37):10774-89.
15. Zadoorian A, Du X, and Yang H. Lipid droplet biogenesis and functions in health and disease. *Nat Rev Endocrinol.* 2023;19(8):443-59.
16. Guo Y, Walther TC, Rao M, Stuurman N, Goshima G, Terayama K, et al. Functional genomic screen reveals genes involved in lipid-droplet formation and utilization. *Nature.* 2008;453(7195):657-61.
17. Borensztajn J, Rone MS, and Kotlar TJ. The inhibition in vivo of lipoprotein lipase (clearing-factor lipase) activity by triton WR-1339. *Biochem J.* 1976;156(3):539-43.
18. Yamazaki T, Sasaki E, Kakinuma C, Yano T, Miura S, and Ezaki O. Increased very low density lipoprotein secretion and gonadal fat mass in mice overexpressing liver DGAT1. *J Biol Chem.* 2005;280(22):21506-14.
19. Marcinkiewicz A, Gauthier D, Garcia A, and Brasaemle DL. The phosphorylation of serine 492 of perilipin a directs lipid droplet fragmentation and dispersion. *J Biol Chem.* 2006;281(17):11901-9.
20. Moon SH, Huang CH, Houlihan SL, Regunath K, Freed-Pastor WA, Morris JPt, et al. p53 Represses the Mevalonate Pathway to Mediate Tumor Suppression. *Cell.* 2019;176(3):564-80 e19.
21. Mordier S, and Iynedjian PB. Activation of mammalian target of rapamycin complex 1 and insulin resistance induced by palmitate in hepatocytes. *Biochem Biophys Res Commun.* 2007;362(1):206-11.
22. Kwon B, and Querfurth HW. Palmitate activates mTOR/p70S6K through AMPK inhibition and hypophosphorylation of raptor in skeletal muscle cells: Reversal by oleate is similar to metformin. *Biochimie.* 2015;118:141-50.

23. Qiu B, Ackerman D, Sanchez DJ, Li B, Ochocki JD, Grazioli A, et al. HIF2alpha-Dependent Lipid Storage Promotes Endoplasmic Reticulum Homeostasis in Clear-Cell Renal Cell Carcinoma. *Cancer Discov.* 2015;5(6):652-67.
24. Thiam AR, Farese RV, Jr., and Walther TC. The biophysics and cell biology of lipid droplets. *Nat Rev Mol Cell Biol.* 2013;14(12):775-86.
25. Pepino MY, Kuda O, Samovski D, and Abumrad NA. Structure-function of CD36 and importance of fatty acid signal transduction in fat metabolism. *Annu Rev Nutr.* 2014;34:281-303.
26. Koizume S, and Miyagi Y. Lipid Droplets: A Key Cellular Organelle Associated with Cancer Cell Survival under Normoxia and Hypoxia. *Int J Mol Sci.* 2016;17(9).

Figure 1

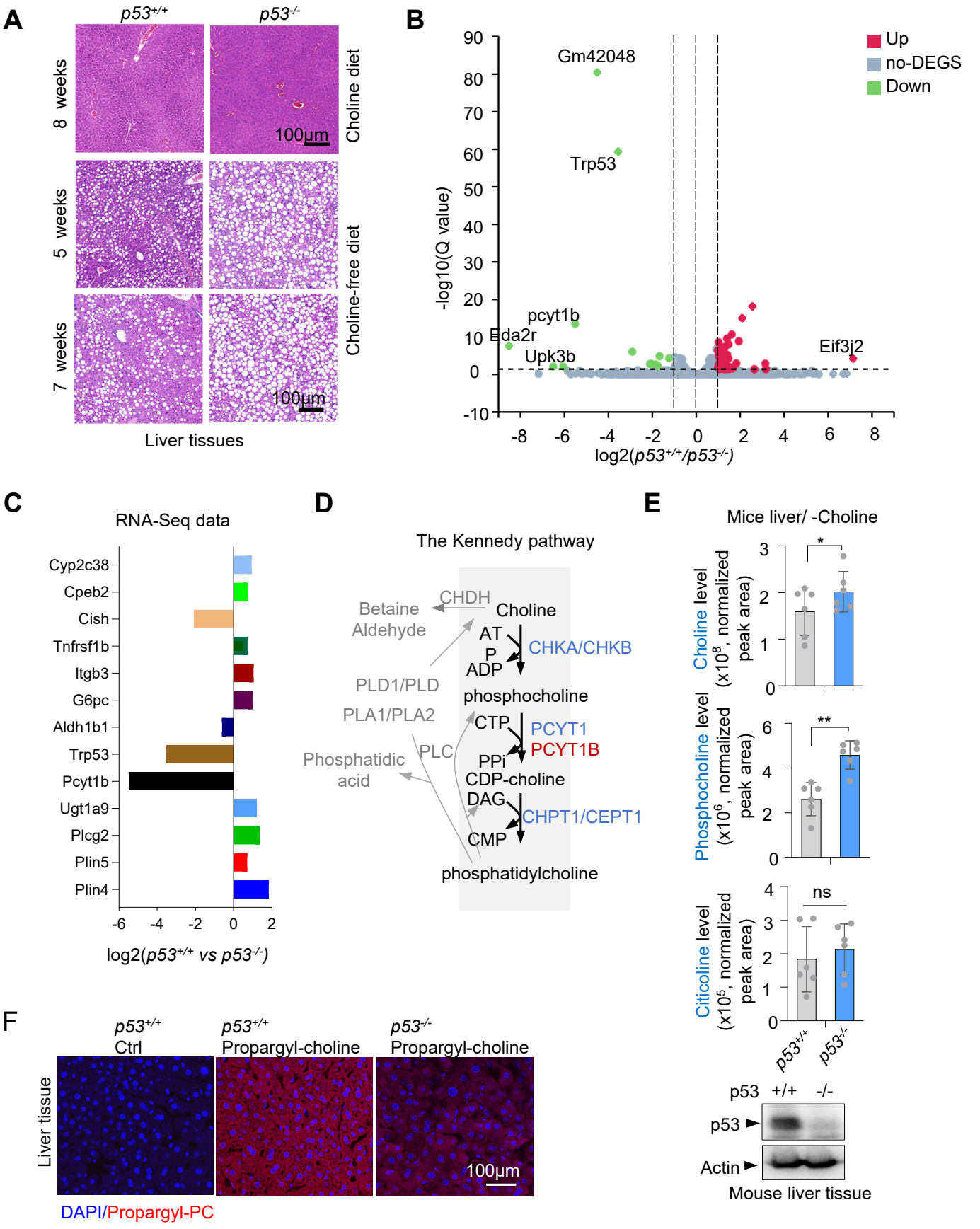
A
p53+/+
p53-/-
8 weeks
5 weeks
7 weeks
Choline diet
Choline-free diet
100μm
100μm
Liver tissues
B
Up
no-DEGS
Down
Gm42048
Trp53
pcyt1b
Eda2r
Upk3b
Eif3j2
-log10(Q value)
log2(p53+/+/p53-/-)
C
RNA-Seq data
Cyp2c38
Cpeb2
Cish
Tnfrsf1b
Itgb3
G6pc
Aldh1b1
Trp53
Pcyt1b
Ugt1a9
Plcg2
Plin5
Plin4
log2(p53+/+ vs p53-/-)
D
The Kennedy pathway
Betaine Aldehyde
CHDH
Choline
ATP
ADP
CHKA/CHKB
phosphocholine
CTP
PPi
PCYT1
PCYT1B
CDP-choline
DAG
CMP
CHPT1/CEPT1
phosphatidylcholine
PLD1/PLD
PLA1/PLA2
PLC
Phosphatidic acid
E
Mice liver/ -Choline
Choline level (x10^8, normalized peak area)
Phosphocholine level (x10^6, normalized peak area)
Citicoline level (x10^5, normalized peak area)
ns
p53+/+
p53-/-
p53 +/+ -/-
p53
Actin
Mouse liver tissue
F
p53+/+ Ctrl
p53+/+ Propargyl-choline
p53-/- Propargyl-choline
Liver tissue
100μm
DAPI/Propargyl-PC

Figure 1. Choline-free diet-associated RNA-seq analysis reveals the Kennedy pathway is downregulated in fatty liver of p53-deficient mice. (**A**) $p53^{+/+}$ and $p53^{-/-}$ mice were maintained on a normal diet for 8 weeks or on a choline-free diet at different time points. Liver tissue from these mice was stained with H&E, n=3 mice per group. (**B** and **C**) RNA-seq of liver tissue from $p53^{+/+}$ and $p53^{-/-}$ mice maintained on a choline-free diet for 4 weeks. (**B**) The volcano plot of log2-fold change of gene expression in the liver tissues between $p53^{+/+}$ and $p53^{-/-}$ mice. Highly up-regulated genes are labeled as red dots, whereas down-regulated ones are labeled in green. (**C**) Bar plot comparison of expression changes of genes involved in lipid metabolism by RNA-seq analysis, n=3 mice per group. (**D**) Schematic depicting the Kennedy (CDP-choline) pathway. (**E**) Normalized LC-MS peak areas of choline, phosphocholine and citicoline in the livers of $p53^{+/+}$ and $p53^{-/-}$ mice maintained on a choline-deficient diets for 5 weeks (n=5 mice per group). p53 expression in liver tissue was determined by western blot analysis. (**F**) $p53^{+/+}$and $p53^{-/-}$ mice maintained on a choline-free diet were teil-vein injected with 0.05 mg/g propargyl-choline for 24 hours or left untreated. The liver tissues were collected and sectioned, and images were acquired on a confocal laser scanning microscope. All data are mean±SD. *P* values were calculated by two-tailed unpaired Student's t-test (**E**). **P*<0.05, ***P*<0.01, ****P*<0.001.

Figure 2

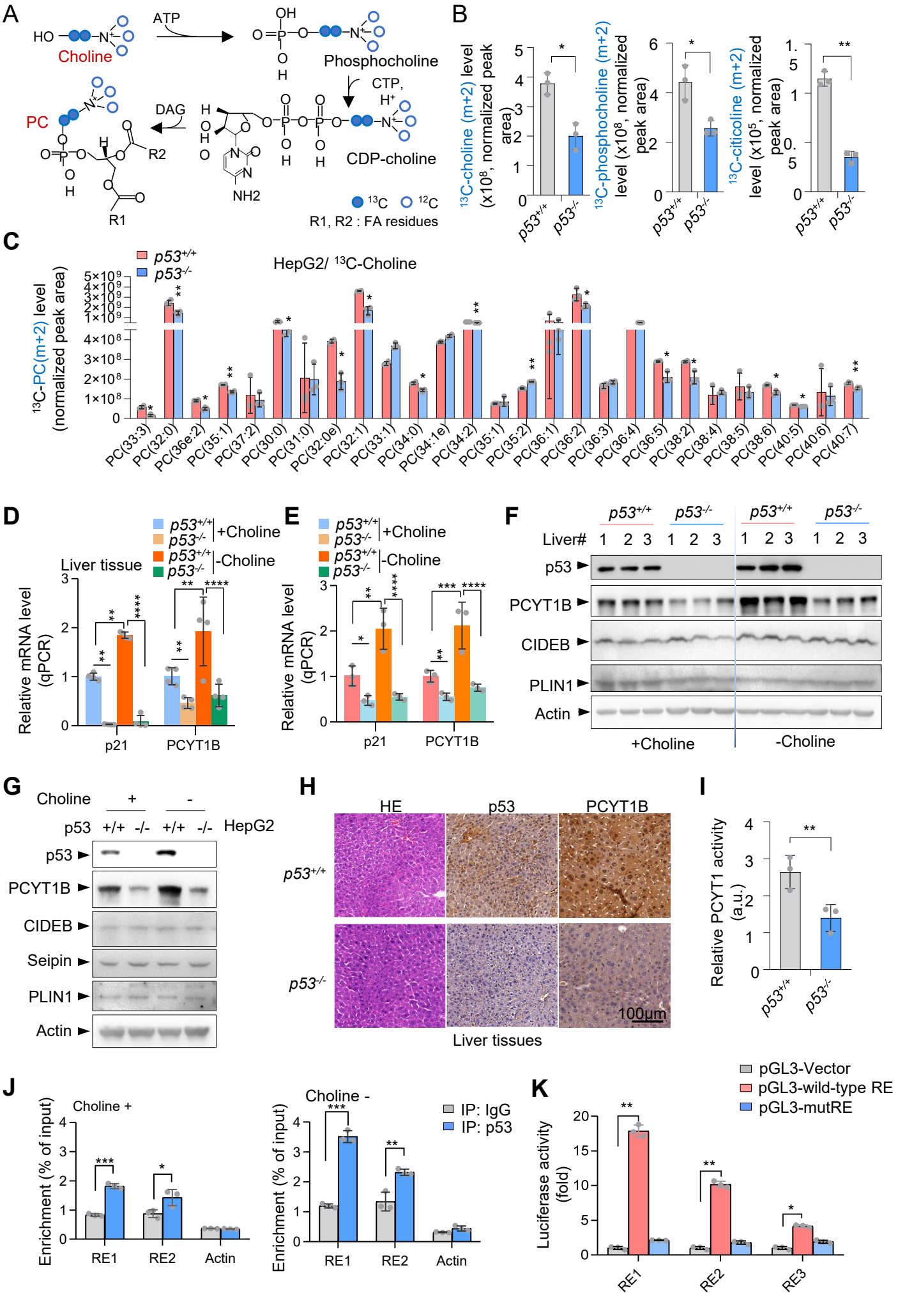
A
Choline
ATP
Phosphocholine
CTP,
CDP-choline
DAG
PC
R1
R2
NH2
13C
12C
R1, R2 : FA residues
B
13C-choline (m+2) level (x10^8, normalized peak area)
13C-phosphocholine (m+2) level (x10^8, normalized peak area)
13C-citicoline (m+2) level (x10^5, normalized peak area)
p53+/+
p53-/-
C
HepG2/ 13C-Choline
13C-PC(m+2) level (normalized peak area)
PC(33:3)
PC(32:0)
PC(36e:2)
PC(35:1)
PC(37:2)
PC(30:0)
PC(31:0)
PC(32:0e)
PC(32:1)
PC(33:1)
PC(34:0)
PC(34:1e)
PC(34:2)
PC(35:1)
PC(35:2)
PC(36:1)
PC(36:2)
PC(36:3)
PC(36:4)
PC(36:5)
PC(38:2)
PC(38:4)
PC(38:5)
PC(38:6)
PC(40:5)
PC(40:6)
PC(40:7)
D
Liver tissue
+Choline
-Choline
Relative mRNA level (qPCR)
p21
PCYT1B
E
Relative mRNA level (qPCR)
p21
PCYT1B
F
Liver#
p53
PCYT1B
CIDEB
PLIN1
Actin
+Choline
-Choline
G
Choline
HepG2
p53
PCYT1B
CIDEB
Seipin
PLIN1
Actin
H
HE
p53
PCYT1B
100μm
Liver tissues
I
Relative PCYT1 activity (a.u.)
J
Choline +
Choline -
IP: IgG
IP: p53
Enrichment (% of input)
RE1
RE2
Actin
K
pGL3-Vector
pGL3-wild-type RE
pGL3-mutRE
Luciferase activity (fold)
RE1
RE2
RE3

Figure 2. p53 drives the Kennedy pathway and transcriptionally upregulates PCYT1B expression. (**A**) Atom-transition map showing the isotope carbon-13 (^{13}C) transfers from [1,2-$^{13}C_2$]-choline through the PC synthetic pathway. Open circles represent carbon-12 (^{12}C), blue circles indicate ^{13}C from [1,2-$^{13}C_2$]-choline. (**B** and **C**) Normalized peak areas of m+2 ^{13}C-labeled metabolites from *p53*$^{+/+}$ and *p53*$^{-/-}$ HepG2 cells cultured with choline-free medium and pulse label with [1,2-$^{13}C_2$]-choline before metabolite extraction. (**B**) ^{13}C-labeled choline, phosphocholine and citicoline. (**C**) ^{13}C-labeled PC. The isotopic labeling of each metabolite is denoted as m+n, where n is the number of ^{13}C atoms. n=3 samples per treatment. (**D** and **F**) *p53*$^{+/+}$ and *p53*$^{-/-}$ mice fed a choline-deficient or a normal diet for 4 weeks (n=3 mice per group). Liver tissues were analyzed by quantitative RT-PCR (**D**) and Western blot (**F**). (**E** and **G**) *p53*$^{+/+}$ and *p53*$^{-/-}$ HepG2 cells cultured in choline-free medium or completed medium were analyzed by quantitative RT-PCR (**E**) and western blot (**G**). (**H**) IHC of mouse liver tissues. The insets are high-magnification views (X20). The scale bar is 100 μm. (**I**) *p53*$^{+/+}$ and *p53*$^{-/-}$ HepG2 cells cultured with [1,2-$^{13}C_2$]-choline for 30 mins and relative PCYT1 activity was determined based on the ratio of CDP-choline and phosphatidylcholine generated. (**J**) Liver tissue from *p53*$^{+/+}$ mice fed a normal or choline-free diet was lysed and immunoprecipitated with anti-p53 or IgG antibody. The bound DNA was amplified by quantitative RT-PCR. (**K**) Luciferase constructs containing wild-type or mutant REs were transfected into HEK93T cells together with Flag-p53 or vector control. Renilla vector pRL-CMV was used as a transfection internal control. Relative luciferase activity was calculated by dividing Flag-p53 samples over the Flag vector control samples. All data are mean±SD. Each experiment was carried out at least 3 independent times. **P*<0.05, ***P*<0.01, ****P*<0.001, *****P*<0.0001. *P* values were calculated by two-tailed unpaired Student's t-test (**B**, **C**, **I**, **J**, and **K**) or two-way ANOVA followed by Tukey's multiple-comparison test (**D** and **E**).

Figure 3

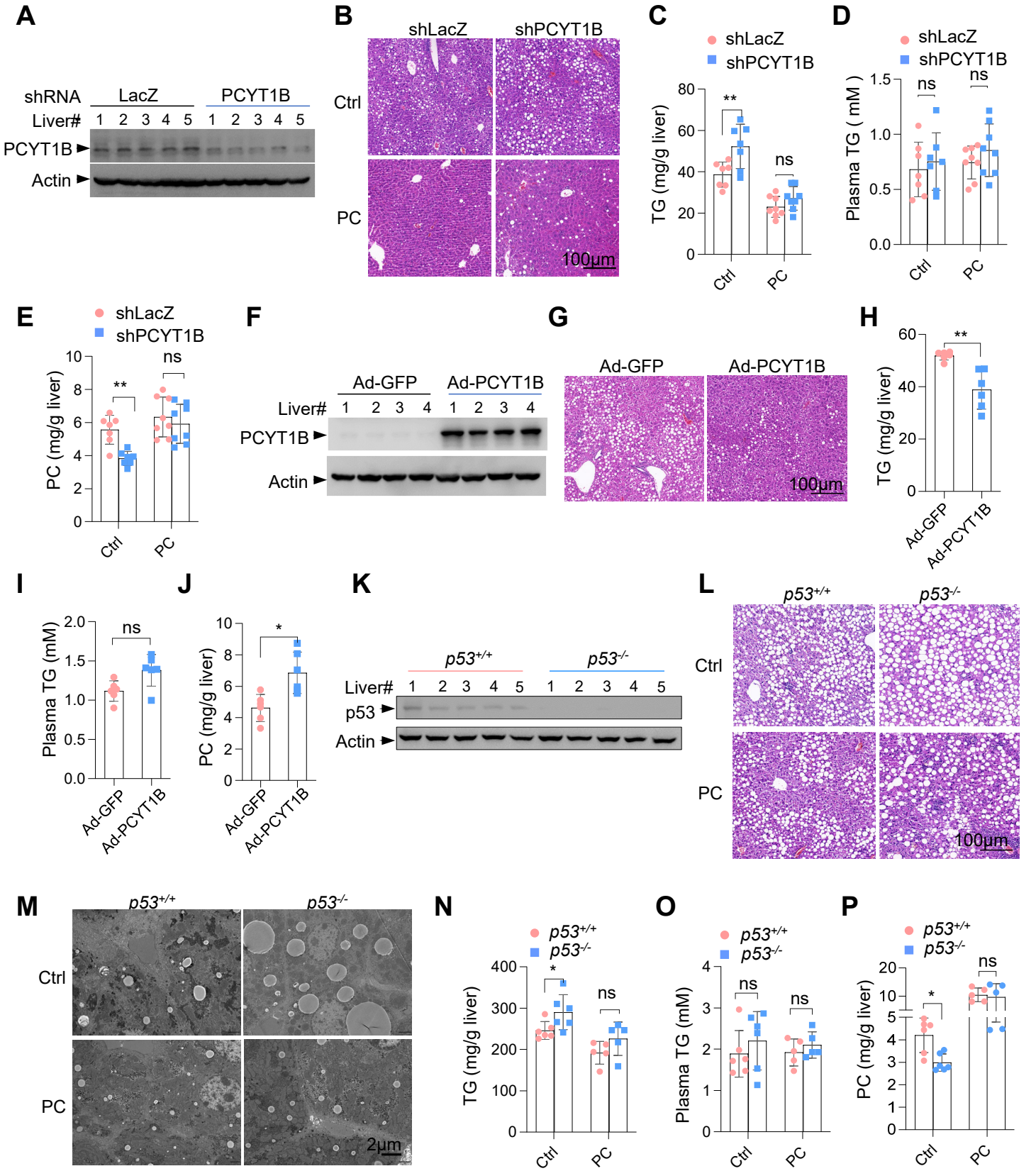
A
shRNA
LacZ
PCYT1B
Liver#
1 2 3 4 5 1 2 3 4 5
PCYT1B
Actin
B
shLacZ
shPCYT1B
Ctrl
PC
100μm
C
shLacZ
shPCYT1B
TG (mg/g liver)
**
ns
Ctrl
PC
D
shLacZ
shPCYT1B
Plasma TG (mM)
ns
ns
Ctrl
PC
E
shLacZ
shPCYT1B
PC (mg/g liver)
**
ns
Ctrl
PC
F
Ad-GFP
Ad-PCYT1B
Liver#
1 2 3 4 1 2 3 4
PCYT1B
Actin
G
Ad-GFP
Ad-PCYT1B
100μm
H
TG (mg/g liver)
**
Ad-GFP
Ad-PCYT1B
I
Plasma TG (mM)
ns
Ad-GFP
Ad-PCYT1B
J
PC (mg/g liver)
*
Ad-GFP
Ad-PCYT1B
K
p53+/+
p53-/-
Liver#
1 2 3 4 5 1 2 3 4 5
p53
Actin
L
p53+/+
p53-/-
Ctrl
PC
100μm
M
p53+/+
p53-/-
Ctrl
PC
2μm
N
p53+/+
p53-/-
TG (mg/g liver)
*
ns
Ctrl
PC
O
p53+/+
p53-/-
Plasma TG (mM)
ns
ns
Ctrl
PC
P
p53+/+
p53-/-
PC (mg/g liver)
*
ns
Ctrl
PC

Figure 3. p53 suppresses hepatic steatosis via the PCYT1B-PC axis in response to choline starvation. (**A**) Mice administrated of shLacZ or shPCYT1B adenoviruses were maintained on a choline-deficient diet, and liver PCYT1B expression was examined. (**B**-**E**) H&E staining (**B**), triglyceride (TG) levels (**C**) and PC abundance (**E**) of the liver tissues from mice adenovirus-administered and feed with choline-deficient diet supplemented with or without 300 μl PC (10 mg/ml). Plasma TG were measured (**D**). n= 7 mice for Ctrl group; n= 8 mice for PC treatment. (**F**) PCYT1B expression in the liver of $p53^{-/-}$ mice administered with control (Ad-GFP) or (Ad-PCYT1B) virus and fed on a choline-free diet. (**G**-**J**) $p53^{-/-}$ mice administered with control (Ad-GFP) or (Ad-PCYT1B) virus were maintained on a choline-free diet. The liver tissues were stained with H&E (**G**). The TG (**H**) and PC abundance (**J**) in the livers, and the plasma TG (**I**) were measured. n=6 mice per group. (**K**) p53 expression in the livers of $p53^{+/+}$ and $p53^{-/-}$ mice maintained on a choline-free diet. (**L** and **M**) H&E staining (**L**) and transmission electron microscopy (TEM)(**M**) imaging of liver tissues from $p53^{+/+}$ and $p53^{-/-}$ mice maintained on a choline-free diet with or without 300 μl PC (10 mg/ml) orally daily. n= 6 mice for Ctrl group; n=5 mice for PC treatment. (**N**-**P**) $p53^{+/+}$ and $p53^{-/-}$ mice were maintained on a choline-free diet with or without oral administration of 300 μL PC (10 mg/ml) daily. Levels of TG (**N**) and PC (**P**) in the liver and the plasma TG (**O**) were examined. n= 6 mice for Ctrl group; n=5 mice for PC treatment. All data are mean±SD. *P<0.05, **P<0.01, ***P<0.001, P values were calculated by two-tailed unpaired Student's t-test (**C**-**E**, **H**-**J**, **N**-**P**).

Figure 4

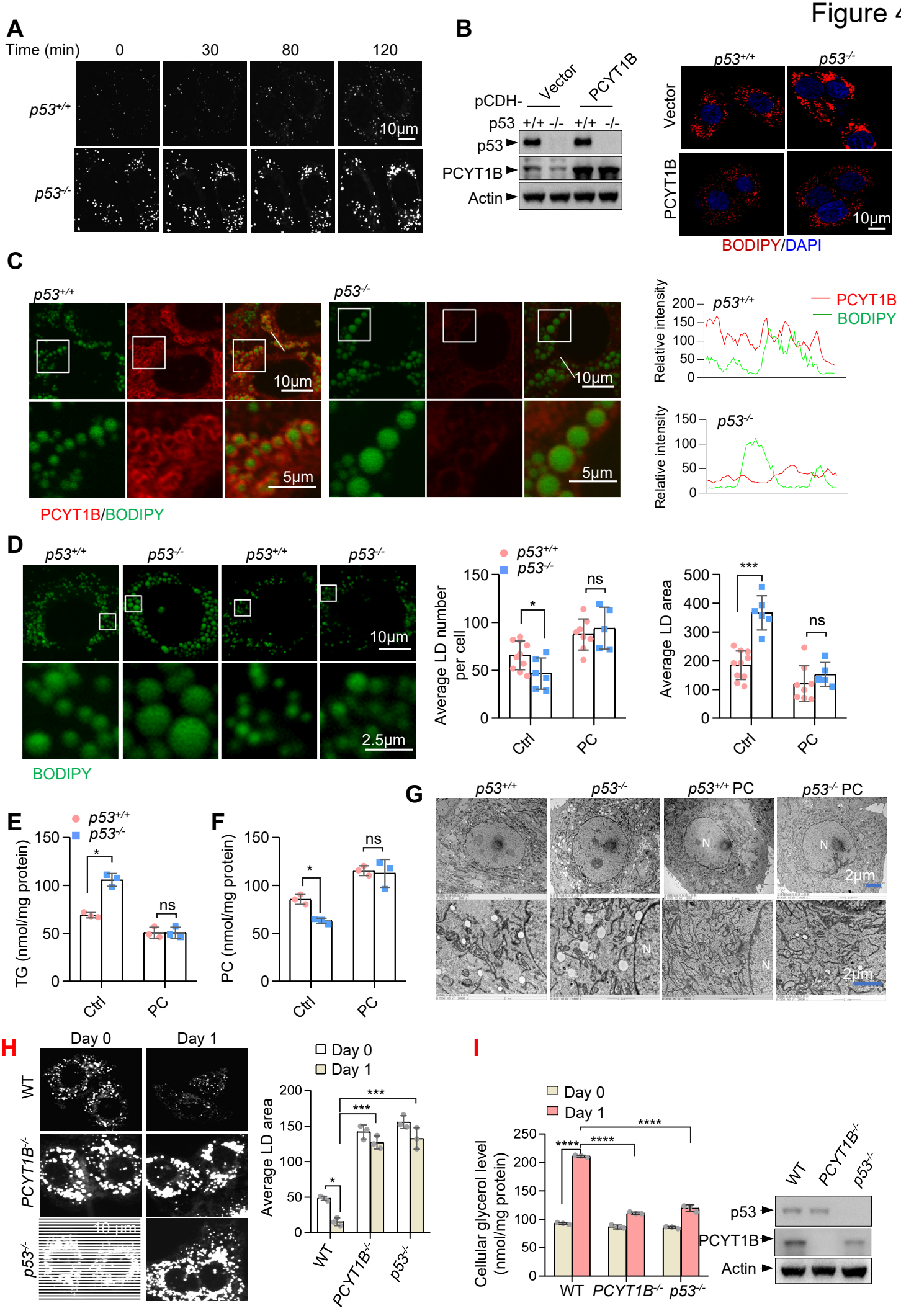
A
Time (min) 0 30 80 120
p53+/+
p53-/-
10μm
B
pCDH- Vector PCYT1B
p53 +/+ -/- +/+ -/-
p53
PCYT1B
Actin
p53+/+ p53-/-
Vector
PCYT1B
10μm
BODIPY/DAPI
C
p53+/+ p53-/-
10μm
5μm
PCYT1B/BODIPY
Relative intensity
PCYT1B
BODIPY
D
p53+/+ p53-/- p53+/+ p53-/-
10μm
2.5μm
BODIPY
Average LD number per cell
Average LD area
Ctrl PC
E
TG (nmol/mg protein)
F
PC (nmol/mg protein)
G
p53+/+ p53-/- p53+/+ PC p53-/- PC
N
2μm
H
Day 0 Day 1
WT
PCYT1B-/-
p53-/-
10 μm
Average LD area
I
Cellular glycerol level (nmol/mg protein)
WT PCYT1B-/- p53-/-
p53
PCYT1B
Actin

Figure 4. p53 regulates LD coalescence via PCYT1B-mediated PC synthesis. (**A**) $p53^{+/+}$ and $p53^{-/-}$ HepG2 cells cultured with 200 μM oleate were stained with BODIPY, and lipid droplet growth was captured with a confocal microscopy at the indicated times. (**B**) $p53^{+/+}$ and $p53^{-/-}$ HepG2 cells stably expressing PCYT1B or vector control were cultured with 200 μM oleate and stained with BODIPY dye and DAPI, and imaged with a confocal microscopy. Expression of PCYT1B was determined by western blot analysis. (**C**) Immunostaining of $p53^{+/+}$ and $p53^{-/-}$ HepG2 cells loaded with 200 μM oleate for 12 hours using PCYT1B antibody or BODIPY 493/503 dye. Enlarged areas are indicated, and the relative intensity of the fluorescence in the specified area of the overlapped images was analyzed (bottom panel). (**D**) $p53^{+/+}$ and $p53^{-/-}$ HepG2 cells cultured in choline-free medium supplemented with or without PC were loaded with 200 μM oleate and stained with BODIPY 493/503 dye. The average numbers and area of LDs were measured. (**E**-**G**) $p53^{+/+}$ and $p53^{-/-}$ HepG2 cells were treated as in (**D**). TG (**E**) and PC (**F**) levels were measured. LDs were imaged with a transmission electron microscopy (**G**). N in (**G**) indicates nucleus. (**H**) Wild-type control, $PCYT1B^{-/-}$ and $p53^{-/-}$ HepG2 cells were loaded with 200 μM oleate for one day. Cells were then imaged by confocal microscopy after staining with BODIPY (day 0, up panels). Oleate was removed from the medium and the cells were starved for one day in serum-free medium to induce lipolysis (day 1, bottom panels). Representative confocal midsections are shown. (**I**) Experiments were as in (**H**), and the cellular glycerol and protein expression was measured. All data are the mean±SD. Each experiment was carried out at least 3 independent times. *P<0.05, **P<0.01, ***P<0.001, ****P<0.0001, P values were calculated by two-tailed unpaired Student's t-test (**D**, **E**, and **F**) or two-way ANOVA followed by Tukey's multiple-comparison test (**H** and **I**).

Figure 5

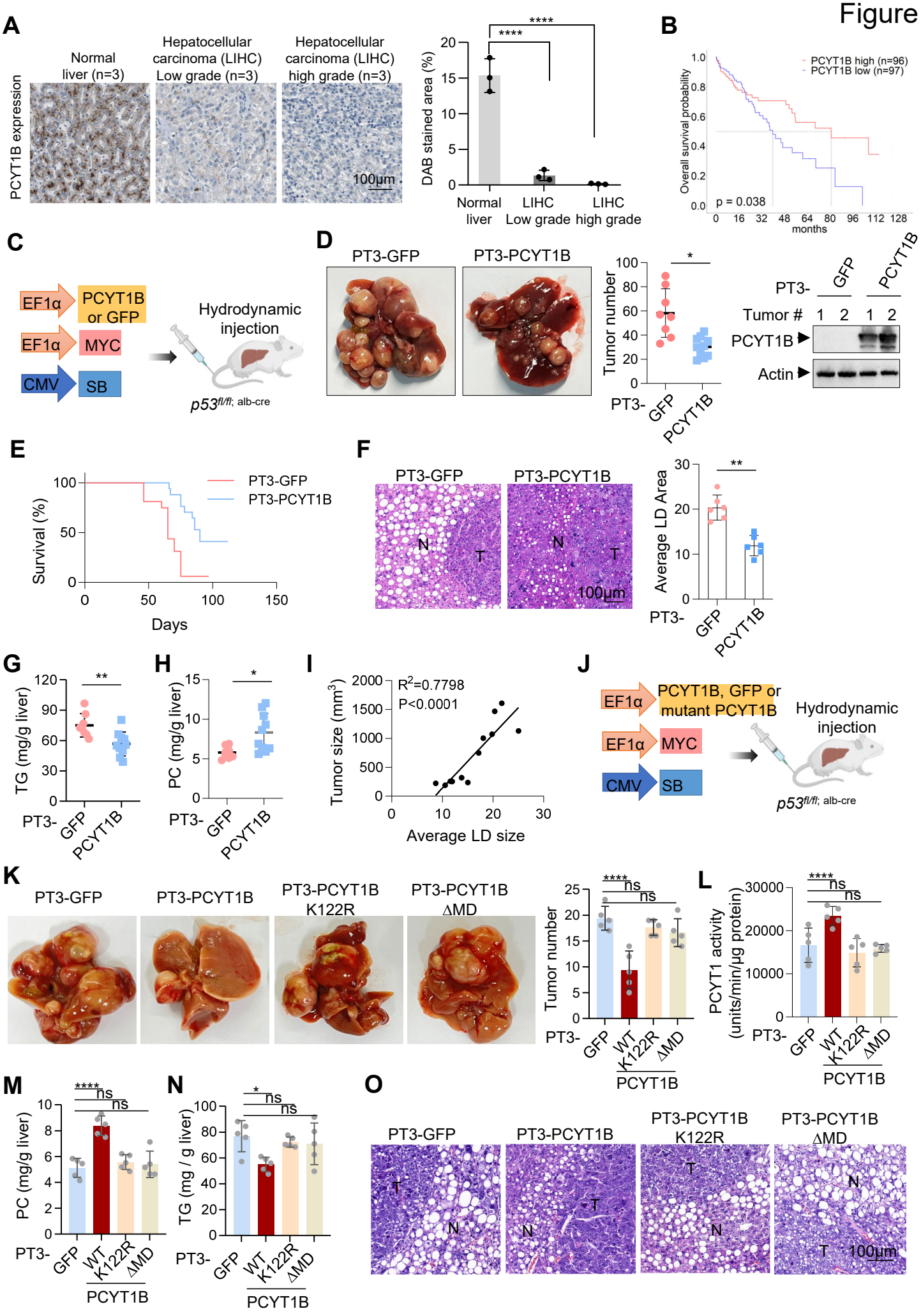
A
Normal liver (n=3)
Hepatocellular carcinoma (LIHC) Low grade (n=3)
Hepatocellular carcinoma (LIHC) high grade (n=3)
PCYT1B expression
100μm
DAB stained area (%)
Normal liver
LIHC Low grade
LIHC high grade
B
PCYT1B high (n=96)
PCYT1B low (n=97)
Overall survival probability
p = 0.038
months
C
EF1α
PCYT1B or GFP
EF1α
MYC
CMV
SB
Hydrodynamic injection
p53fl/fl; alb-cre
D
PT3-GFP
PT3-PCYT1B
Tumor number
PT3-
GFP
PCYT1B
Tumor #
Actin
E
PT3-GFP
PT3-PCYT1B
Survival (%)
Days
F
PT3-GFP
PT3-PCYT1B
N
T
100μm
Average LD Area
G
TG (mg/g liver)
H
PC (mg/g liver)
I
R2=0.7798
P<0.0001
Tumor size (mm3)
Average LD size
J
EF1α
PCYT1B, GFP or mutant PCYT1B
EF1α
MYC
CMV
SB
Hydrodynamic injection
p53fl/fl; alb-cre
K
PT3-GFP
PT3-PCYT1B
PT3-PCYT1B K122R
PT3-PCYT1B ΔMD
Tumor number
WT
K122R
ΔMD
PCYT1B
L
PCYT1 activity (units/min/μg protein)
M
PC (mg/g liver)
N
TG (mg / g liver)
O
PT3-GFP
PT3-PCYT1B
PT3-PCYT1B K122R
PT3-PCYT1B ΔMD
100μm

Figure 5. PCYT1B is a metabolic tumor suppressor. (**A**) Expression of PCYT1B in normal liver tissues and carcinoma of different stages was determined by immunohistochemistry (proteinatlas.org). Magnified regions of PCYT1B staining are provided. (**B**) Kaplan–Meier survival curves of patients with liver cancer based on PCYT1B expression. Grey dotted lines mine median survival time. (**C-I**) PCYT1B suppresses liver tumorigenesis in response to oncogenic stress in $p53^{fl/fl;alb\text{-}cre}$ mice. (**C**) Diagram depicting generation of liver tumor models. (**D,** right) Representative expression of PCYT1B in tumors. (**D,** left) Representative images of liver tumor multiplicity and the number of tumors. n=8 (for PT3-GFP injection) or 10 (for PT3-PCYT1B injection) mice per group. (**E**) Kaplan-Meier survival curves of $p53^{fl/fl;\ alb\text{-}cre}$ mouse HTVI with transposons expressing MYC and PCYT1B (GFP). n=16 for GFP group; n=17 for PCYT1B group. **(F)** Representative histological analysis of the tumors stained for H&E. Images and quantification were taken at tumor periphery. The levels of liver TG (**G**) and PC (**H**) were measured. Linear regression analysis was performed on the mean LD size and tumor size in the murine livers (**I**) (n =12). **(J-O)** (**J**) $p53^{fl/fl;alb\text{-}cre}$ mice were fed on a choline-free diet 6 weeks after injection with the components as indicated using HTVI. (**K**) Representative images and the number of liver tumors. (**L**) The liver tumor tissue PCYT1 activity. Absolute levels of PC (**M**) and TG (**N**) in the livers were measured. (**O**) Representative histological analysis of the tumors stained for H&E. n=5 for per group. All data are mean±SD. Each experiment was carried out at least 3 independent times. **P*<0.05, ***P*<0.01, ****P*<0.001, *****P*<0.0001, n.s., not statistical significance. *P* values were calculated by two-tailed unpaired Student's t-test (**A**, **D**, **F**, **G** and **H**) or two-way ANOVA followed by Dunnett's multiple-comparison test (**K**, **L**, **M** and **N**) or by linear regression analysis (**I**) or by log-rank (Mantel-Cox) test (**B** and **E**).

Figure 6

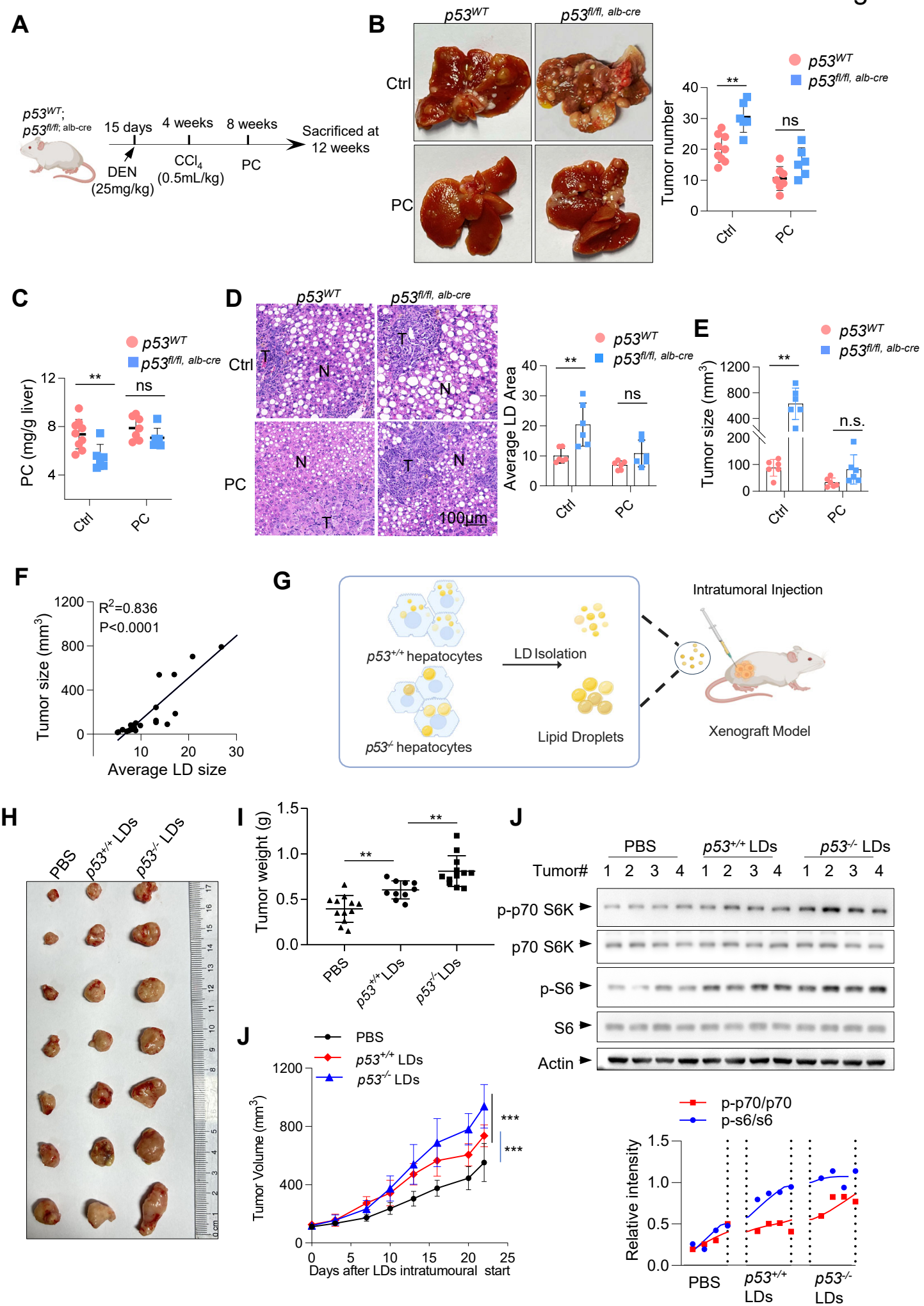
A
p53WT; p53fl/fl; alb-cre
15 days
4 weeks
8 weeks
Sacrificed at 12 weeks
DEN (25mg/kg)
CCl4 (0.5mL/kg)
PC
B
p53WT
p53fl/fl, alb-cre
Ctrl
PC
Tumor number
ns
C
PC (mg/g liver)
D
T
N
100μm
Average LD Area
E
Tumor size (mm3)
n.s.
F
R2=0.836
P<0.0001
Average LD size
G
p53+/+ hepatocytes
LD Isolation
p53-/- hepatocytes
Lipid Droplets
Intratumoral Injection
Xenograft Model
H
PBS
p53+/+ LDs
p53-/- LDs
I
Tumor weight (g)
J
Tumor Volume (mm3)
Days after LDs intratumoural start
Tumor#
p-p70 S6K
p70 S6K
p-S6
S6
Actin
p-p70/p70
p-s6/s6
Relative intensity

Figure 6. Downregulation of the Kennedy pathway is required for the development of liver tumors harboring p53 loss. $p53^{WT}$ and $p53^{fl/fl;alb\text{-}cre}$ mice were treated with DEN, CCl_4, PC and fed on a choline-free diet, as illustrated in (**A**). (**B**) The number of liver tumors was measured at week 12 (**B**, right) and representative images of liver tumor multiplicity are shown (**B**, left). n = 9 (for control $p53^{WT}$ mice), 6 (for PC-treated $p53^{WT}$ mice), 7 (for control $p53^{fl/fl;alb\text{-}cre}$ mice), or 6 (for PC-treated $p53^{fl/fl;alb\text{-}cre}$ mice) mice per group. (**C**) Absolute levels of PC in the livers were measured. (**D**) Representative histological analysis of the tumors stained for H&E, and the LD area were quantified. Images and quantification were taken at tumor periphery. (**E**)The tumor size was assessed. (**F**) Linear regression analysis was performed on the mean LD size and tumor size in the murine livers (n = 24). (**G**-**K**) Lipid droplets isolated and purified from the equal amount of liver tissues from $p53^{WT}$ and $p53^{fl/fl;alb\text{-}cre}$ mice fed on a choline-free diet were injected into the transplanted tumor derived from HepG2 cells in NCG mice in twice a week as illustrated in (**G**). (**H**) Representative images of the transplanted tumors. (**I**) Average weights of xenograft tumors on day 22 (n= 12 tumors for PBS group; n= 10 tumors for $p53^{+/+}$ LDs group; n= 12 tumors for $p53^{-/-}$ LDs group). (**J**)Tumor volume. (**K**) Tumors were analyzed by Western blot. All data are mean±SD. Each experiment was carried out at least 3 independent times. *P<0.05, **P<0.01, ***P<0.001, n.s., not statistical significance. P values were calculated by two-tailed unpaired Student's t-test (**B**-**E**) or two-way ANOVA followed by Sidak's multiple-comparison test (I) or by linear regression analysis (**F**) or two-way ANOVA (**J**).

Figure 7

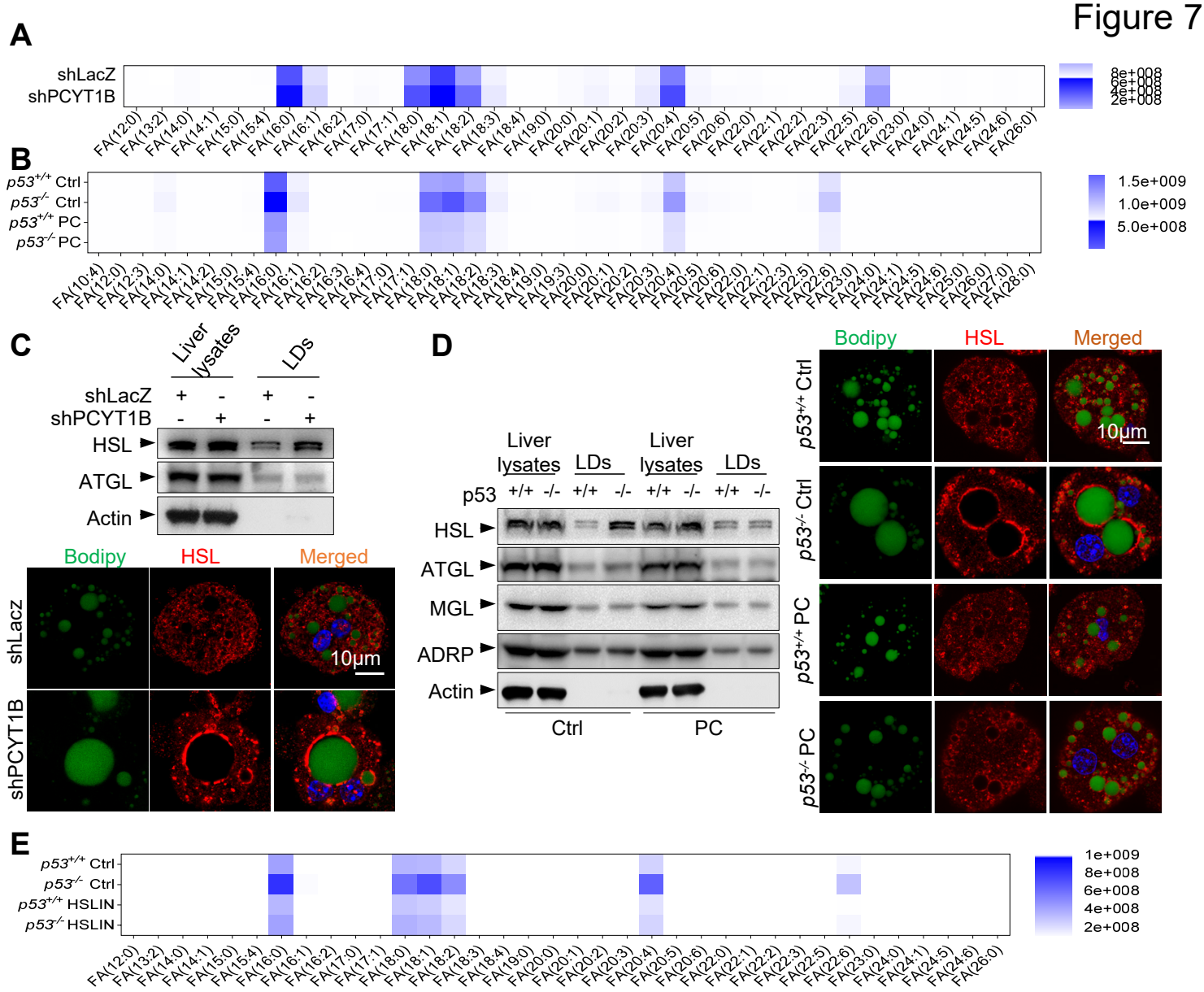
A
shLacZ
shPCYT1B
8e+008
6e+008
4e+008
2e+008
B
p53+/+ Ctrl
p53-/- Ctrl
p53+/+ PC
p53-/- PC
1.5e+009
1.0e+009
5.0e+008
C
Liver lysates
LDs
shLacZ
shPCYT1B
HSL
ATGL
Actin
Bodipy
HSL
Merged
shLacz
shPCYT1B
10μm
D
Liver lysates
LDs
p53
HSL
ATGL
MGL
ADRP
Actin
Ctrl
PC
Bodipy
HSL
Merged
p53+/+ Ctrl
p53-/- Ctrl
p53+/+ PC
p53-/- PC
10μm
E
p53+/+ Ctrl
p53-/- Ctrl
p53+/+ HSLIN
p53-/- HSLIN
1e+009
8e+008
6e+008
4e+008
2e+008
F
p53+/+
p53-/-
Vector
HSL gRNA
Tumor number
**
ns
G
Vector
HSL gRNA
Liver tumor#
p53
HSL
p-p70 S6K
p70 S6K
p-S6
S6
Actin
H
p53+/+
p53-/-
Vector
HSL gRNA
T
N
100μm
I
Hepatocyte -cultured medium
p53+/+ Ctrl
p53-/- Ctrl
p53+/+ HSLIN
p53-/- HSLIN
p53+/+ HSLIN,+OA(C18:1)
OD450 values
Days
***
***
J
Hepatocyte -cultured medium
Ctrl
HSLIN
p53
OA (18:1)
p-p70 S6K
p-p70/p70:
p70 S6K
p-S6
p-S6/S6:
S6
Actin
HepG2

Figure 7. Suppression of PC biosynthesis by p53 loss increases surface localization of HSL to release specific FAs as fuel for tumorigenesis. (**A** and **C**) Mice treated with shLacZ or shPCYT1B adenoviruses were maintained on a choline-deficient diet. (**A**) Fatty acid levels in the interstitial fluid of liver tissue. (**C**) Liver tissues and purified liver LDs were analyzed by Western blot, and isolated hepatocytes were immunostained as indicated. (**B** and **D**) $p53^{+/+}$ and $p53^{-/-}$ mice were maintained on a choline-free diet with or without oral administration of 300 μL PC (10 mg/ml) daily. (**B**) Fatty acid levels in the interstitial fluid of liver tissue. (**D**) Liver tissue and purified liver LDs were analyzed by Western blot and isolated hepatocytes were immunostained as indicated. (**E**) The levels of fatty acids in liver tissue interstitial fluid from $p53^{+/+}$ and $p53^{-/-}$ mice maintained on a choline-free diet with or without oral administration of 100 μL HSL inhibitor (HSL-IN-1, 5 mg/ml) daily. (**F**-**H**) The experimental procedures are illustrated in Supplemental Figure 15**E**. (**F**) Representative images of liver tumor multiplicity and the number of tumors. (**G**) Liver tissues were analyzed by Western blot. (**H**) Representative histological analysis of H&E-stained tumors. n=6 mice per group. (**I** and **J**) $p53^{+/+}$ and $p53^{-/-}$ mice were maintained on a choline-free diet with or without oral administration of 100 μL HSL inhibitor (5 mg/ml) daily. The isolated hepatocytes were cultured in lipid-free medium and the conditioned medium containing no or 50 μM oleate was then used to culture HepG2 cells for different times. HepG2 cell proliferation and mTORC1 activity were determined. All data are mean±SD. Each experiment was carried out at least 3 independent times. ***P<0.001, n.s., not statistical significance. P values were calculated by two-tailed unpaired Student's t-test (**F**) or two-way ANOVA (**I**).